The Astronomical Journal, 142:88 (12pp), 2011 September doi:10.1088/0004-6256/142/3/88

SEGUE 3: AN OLD, EXTREMELY LOW LUMINOSITY STAR CLUSTER IN THE MILKY WAY'S HALO

Ross Fadely[1], Beth Willman[1], Marla Geha[2], Shane Walsh[3,6], Ricardo R. Muñoz[2,4], Helmut Jerjen[5], Luis C. Vargas[2], and Gary S. Da Costa[5]

[1] Department of Astronomy, Haverford College, Haverford, PA 19041, USA; rfadely@haverford.edu, bwillman@haverford.edu

[2] Astronomy Department, Yale University, New Haven, CT 06520, USA

[3] Australian Astronomical Observatory/Las Campanas Observatory, La Serena, Chile

[4] Departamento de Astronomía, Universidad de Chile, Casilla 36-D, Santiago, Chile

[5] Research School of Astronomy & Astrophysics, Australian National University, Canberra, Australia

Received 2011 June 22; accepted 2011 July 15; published 2011 August 16

ABSTRACT

We investigate the kinematic and photometric properties of the Segue 3 Milky Way companion using Keck/DEIMOS spectroscopy and Magellan/IMACS *g*- and *r*-band imaging. Using maximum likelihood methods to analyze the photometry, we study the structure and stellar population of Segue 3. We find that the half-light radius of Segue 3 is $26' \pm 5'$ (2.1 ± 0.4 pc, for a distance of 17 kpc) and the absolute magnitude is a mere $M_V = 0.0 \pm 0.8$ mag, making Segue 3 the least luminous old stellar system known. We find Segue 3 to be consistent with a single stellar population, with an age of $12.0^{+1.5}_{-0.4}$ Gyr and an [Fe/H] of $-1.7^{+0.07}_{-0.27}$. Line-of-sight velocities from the spectra are combined with the photometry to determine a sample of 32 stars which are likely associated with Segue 3. The member stars within three half-light radii have a velocity dispersion of 1.2 ± 2.6 km s^{-1}. Photometry of the members indicates that the stellar population has a spread in [Fe/H] of $\lesssim$0.3 dex. These facts, together with the small physical size of Segue 3, imply the object is likely an old, faint stellar cluster which contains no significant dark matter. We find tentative evidence for stellar mass loss in Segue 3 through the 11 candidate member stars outside of three half-light radii, as expected from dynamical arguments. Interpretation of the data outside of three half-light radii is complicated by the object's spatial coincidence with a previously known halo substructure, which may enhance contamination of our member sample.

Key words: galaxies: dwarf – galaxies: star clusters: general – Galaxy: kinematics and dynamics – globular clusters: individual (Segue 3)

Online-only material: color figures

1. INTRODUCTION

Segue 3 (hereafter Seg 3) is a recently discovered Milky Way satellite, initially estimated to have an extremely low luminosity ($M_V \sim -1.2$, $\sim$250 $L_\odot$), a half-light radius of $\sim$3 pc, and a distance of $\sim$17 kpc (Belokurov et al. 2010). Five other Milky Way satellites are known to have comparably small luminosities and scale sizes: Whiting 1 ($M_V = -2.46$), Pal 1 ($M_V = -2.52$), AM 4 ($M_V \sim -1.8$), Koposov 1 ($M_V = -1.35$), and Koposov 2 ($M_V \sim -0.35$; Harris 1996, 2010 edition). All six of these objects are relative outliers in size and luminosity from other known Milky Way satellites, with luminosities a factor of three lower than those of the other 112 Milky Way satellites with half-light radii smaller than 5 pc.

These six extreme satellites lie at distances ranging from 17 kpc (Segue 3, Pal 1) to 40 kpc or more (Koposov 1 and 2). Despite these halo distances, one explanation for their anomalously low luminosities is stellar mass loss owing to dynamical evolution, such as tidal stripping or tidal shocking. At their current stellar masses and sizes, the evaporation timescales of these clusters are also shorter than the observed ages of the systems (see, e.g., discussion in Koposov et al. 2007), suggesting that evaporation is playing a major role in their evolution. The hypothesis that these satellites are experiencing substantial stellar mass loss is supported by observations: strong evidence for extra-tidal stars has been found in Pal 1, AM 4, and Whiting 1 (Carraro 2009; Carraro et al. 2007; Niederste-Ostholt et al. 2010). (Koposov 1 and 2 have not yet been studied thoroughly enough to confirm or rule out the presence of extra-tidal stars.) Most of these six ultra-low-luminosity satellites have been (at least tentatively) associated with larger scale stellar streams in the halo. For example, Whiting 1 and Koposov 1 have been associated with the Sgr stream (Carraro et al. 2007; Koposov et al. 2007), AM 4 possibly with the Sgr stream (Carraro 2009), Pal 1 possibly with the Galactic Anticenter Stellar Structure (GASS; Frinchaboy et al. 2004) or Canis Major (Forbes & Bridges 2010), and Segue 3 possibly with the Hercules–Aquila cloud (Belokurov et al. 2010).

Perhaps all six of these $M_V > -2.5$, $r_{1/2} < 5$ pc satellites are stripped down versions of more luminous objects, and can provide insight into the evolution of the Milky Way's satellite population and into the buildup of the halo. Because of their small physical sizes and luminosities alone, they have all been classified as globular clusters in the literature. Their central surface brightnesses are higher than those of the known Milky Way dwarfs, so they are not simply stripped versions of those objects. Although this circumstantial evidence supports a model where these outliers may instead be stripped versions of more luminous globular clusters, no robust classification or detailed kinematic study of these objects has yet been done.

We aim to improve our understanding of these unusual Milky Way satellites by conducting a detailed kinematic study of Segue 3, the first to be done for any comparable object. In particular, we study Magellan/IMACS photometry in *g* and *r* of Segue 3 to investigate its structural parameters and star formation history. We combine this photometry with Keck/DEIMOS spectroscopy

[6] Magellan Fellow.

to obtain a robust member sample. We use these spectroscopic members to study Seg 3's internal kinematics and to look for evidence of the extra-tidal stars seen in similar clusters. We use its internal kinematics, improved structural parameters, and star formation history to infer a star cluster classification for Seg 3.

2. DATA

2.1. Photometry

We observed Segue 3 using Magellan/IMACS during engineering time on 2010 August 21 with bright conditions and excellent ∼0.″3 seeing. We used the IMACS in $f/4$ mode, giving a pixel scale of 0.″111 pixel^{-1} and a 15.′5 × 15.′5 field of view. We obtained a total integration time of 1620 s in each of the g and r Sloan filters, using observations which were dithered across the sky.

Individual chip images were reduced and stacked to create a weighted mosaic using `SExtractor`, `SCAMP`, and `SWarp` (Bertin & Arnouts 1996; Bertin et al. 2002; Bertin 2006), with Sloan Digital Sky Survey Data Release 7 (SDSS DR7) providing the astrometric calibration. Normalized flats were used to weight the images, with zero weightings given for known defects. The stacked mosaics were then photometered using the stand-alone `DAOPHOT II/Allstar` package (Stetson 1987).

The photometry was calibrated to SDSS by astrometrically matching the stars and then fitting for the difference between instrumental and SDSS magnitudes and colors. To robustly determine the calibration parameters, we used a 1000 iteration bootstrap method which calibrated our detections to SDSS sources within our region of interest in the color–magnitude diagram (CMD): sources with g and r magnitudes between 18.0 and 22.5, and $0.1 < g - r < 0.5$. For each iteration, we first use an iterative 3σ clip to remove outliers and then do an uncertainty weighted fit for the zero points and color terms. We adopt the median values of the bootstrap analysis for the calibration, along with their standard deviations. The calibration we determine is

$$g = g_{\rm inst} + 1.588 \pm 0.017 - 0.079 \pm 0.016(g_{\rm inst} - r_{\rm inst}),$$
$$r = r_{\rm inst} + 1.887 \pm 0.014 - 0.018 \pm 0.017(g_{\rm inst} - r_{\rm inst}).$$

After calibration, we conducted Monte Carlo tests to assess the completeness of our photometric data. Specifically, completeness limits were calculated by injecting the mosaic image with a 250 × 250 grid of artificial stars, spaced 30 pixels apart in x and y directions plus a small random offset. We repeated this injection 24 times for a total of 1,500,000 artificial stars in each filter. For each star, we randomly assign a magnitude between 18 and 25 and subsequently detected the stars using the same criteria as the real data. We set valid detections as those with a position within 1 pixel of the input position, and measure the fraction recovered as a function of magnitude. We find that the 90% completion limits for our g- and r-band data are 23.7 and 23.9, respectively.

2.2. Spectroscopy

The spectroscopic data were taken with the Keck II 10 m telescope and the DEIMOS spectrograph (Faber et al. 2003). To select spectroscopic targets, we used the SDSS DR7 photometry, because the IMACS photometry discussed in Section 2.1 was not available at the time. Candidate Segue 3 member stars were identified by comparison to a Padua theoretical isochrone for an age of 13 Gyr and a metallicity of [Fe/H]= −2.3 (Marigo et al. 2008). Stars within 0.1 mag of this isochrone and brighter than $r = 22$ were given the highest priority for spectroscopy; stars within 0.2 mag of the isochrone were given lower priority, all other stars observed were selected in order to fill in the mask. Slit masks were created using the DEIMOS `dsimulator` slit mask design software.

Two Keck/DEIMOS multislit masks were observed on 2009 November 16 and a third mask on 2010 May 16. The masks were observed for one hour each with the 1200 line mm^{-1} grating covering a wavelength region 6400–9100 Å. The spectral dispersion of this setup is 0.33 Å, and the resulting spectral resolution, taking into account the anamorphic distortion, is 1.37 Å (FWHM, equivalent to 47 km s^{-1} at the Ca II triplet). The spatial scale is 0.″12 pixel^{-1} and slitlets were 0.″7 wide. The minimum slit length was 4″ which allows adequate sky subtraction; the minimum spatial separation between slit ends was 0.″4 (3 pixels).

Spectra were reduced using a modified version of the `spec2d` software pipeline (version 1.1.4) developed by the DEEP2 team at the University of California-Berkeley for that survey. A detailed description of the reductions can be found in Simon & Geha (2007). The final one-dimensional (1D) spectra are rebinned into logarithmic wavelength bins with 15 km s^{-1} pixel^{-1}. Radial velocities were measured by cross-correlating the observed science spectra with a series of high signal-to-noise stellar templates. We calculate and apply a telluric correction to each science spectrum by cross-correlating a hot stellar template with the night sky absorption lines following the method in Sohn et al. (2007). The telluric correction accounts for the velocity error due to mis-centering the star within the 0.″7 slit caused by small mask rotations or astrometric errors. We apply both a telluric and heliocentric correction to all velocities presented in this paper.

We determine the random component of our velocity errors using a Monte Carlo bootstrap method. Noise is added to each pixel in the 1D science spectrum, we then recalculate the velocity and telluric correction for 1000 noise realizations. Error bars are defined as the square root of the variance in the recovered mean velocity in the Monte Carlo simulations. The systematic contribution to the velocity error was determined by Simon & Geha (2007) to be 2.2 km s^{-1} based on repeated independent measurements of individual stars. The systematic error contribution is expected to be constant as the spectrograph setup and velocity cross-correlation routines are identical. We add the random and systematic errors in quadrature to arrive at the final velocity error for each science measurement. Radial velocities were successfully measured for 163 of the 205 extracted spectra across. The fitted velocities were visually inspected to ensure reliability. Our final sample consists of 149 measurements of 132 unique stars, presented in Tables 1 and 2. Of the 17 stars with repeat measurements, we identify one binary star candidate (ID 9, Table 1), with velocities which differ by more than 3σ between observation epochs. The remaining stars exhibit velocities consistent within 2σ. For our analysis below, we use a combined velocity for all stars with repeat measurements, but exclude the identified binary when calculating the velocity dispersion of Seg 3.

3. A SPECTROSCOPIC SAMPLE OF SEGUE 3 STARS

We combine our photometric and spectroscopic data to determine probable members of Seg 3. In Figure 1 we present

Table 1
Photometric and Kinematic Data for Keck/DEIMOS Sample—I. Candidate Members

ID	Date (yyyy-mm-dd)	α (J2000) (h m s)	δ (J2000) ($^\circ$ $'$ $''$)	Radial Distance ($'$)	r (mag)	$(g-r)$ (mag)	$v_{\rm helio}$ (km s^{-1})
1	2009-11-16	21:21:31.4	+19:07:00.3	0.11	20.1	0.23	-162.0 ± 4.5
2	Combined	21:21:31.5	+19:07:04.0	0.11	20.2	0.22	-158.9 ± 3.2
	2009-11-16						-179.3 ± 10.6
	2010-05-16						-157.9 ± 3.2
3	2009-11-16	21:21:31.5	+19:07:09.6	0.17	20.7	0.25	-160.9 ± 7.6
4	2009-11-16	21:21:30.3	+19:06:58.5	0.18	20.0	0.22	-170.0 ± 3.8
5	Combined	21:21:30.4	+19:07:13.4	0.23	21.2	0.30	-168.9 ± 5.4
	2009-11-16						-168.7 ± 6.8
	2010-05-16						-169.2 ± 8.0
6	2009-11-16	21:21:29.9	+19:07:07.7	0.28	20.6	0.23	-153.3 ± 5.9
7	2010-05-16	21:21:30.0	+19:06:52.2	0.28	21.9	0.41	-171.3 ± 9.6
8	Combined	21:21:30.3	+19:06:45.6	0.32	20.4	0.22	-167.6 ± 4.7
	2009-11-16						-170.1 ± 9.1
	2010-05-16						-166.1 ± 5.2
9	Combined	21:21:32.7	+19:06:57.4	0.42	20.5	0.27	-161.2 ± 3.1
	2009-11-16						-176.3 ± 3.8
	2010-05-16						-146.3 ± 3.8
10	2009-11-16	21:21:29.4	+19:07:12.5	0.42	19.8	0.20	-163.2 ± 3.0
11	2010-05-16	21:21:29.0	+19:07:19.6	0.56	22.1	0.49	-172.5 ± 7.8
12	2009-11-16	21:21:29.8	+19:07:30.4	0.56	21.1	0.28	-175.7 ± 6.3
13	Combined	21:21:33.1	+19:06:40.3	0.61	20.5	0.23	-166.1 ± 4.2
	2009-11-16						-155.7 ± 11.3
	2010-05-16						-167.4 ± 4.4
14	2009-11-16	21:21:30.8	+19:06:21.5	0.68	20.4	0.23	-155.2 ± 4.0
15	2009-11-16	21:21:31.1	+19:07:51.9	0.83	19.4	0.28	-163.5 ± 2.8
16	2009-11-16	21:21:32.7	+19:07:47.9	0.86	21.6	0.38	-169.9 ± 5.3
17	Combined	21:21:33.6	+19:06:23.8	0.88	20.0	0.22	-162.7 ± 2.7
	2009-11-16						-158.6 ± 3.3
	2010-05-16						-165.4 ± 3.0
18	2010-05-16	21:21:29.1	+19:06:15.3	0.89	21.2	0.33	-167.7 ± 4.6
19	2009-11-16	21:21:27.1	+19:07:12.5	0.94	21.4	0.32	-165.3 ± 3.6
20	Combined	21:21:26.4	+19:06:35.6	1.18	20.4	0.25	-182.4 ± 3.0
	2009-11-16						-184.6 ± 4.0
	2010-05-16						-181.1 ± 3.8
21	Combined	21:21:31.0	+19:08:16.6	1.24	20.5	0.24	-166.6 ± 3.4
	2009-11-16						-167.7 ± 4.5
	2010-05-16						-165.9 ± 4.0
22	Combined	21:21:38.1	+19:07:33.5	1.75	21.7	0.36	-183.1 ± 4.7
	2009-11-16						-167.9 ± 10.8
	2010-05-16						-186.0 ± 5.1
23	Combined	21:21:32.0	+19:08:52.5	1.86	21.2	0.31	-167.6 ± 4.5
	2009-11-16						-158.5 ± 11.4
	2010-05-16						-168.8 ± 4.7
24	Combined	21:21:36.2	+19:08:27.2	1.88	21.6	0.36	-166.8 ± 5.5
	2009-11-16						-162.4 ± 6.2
	2010-05-16						-180.7 ± 10.6
25	2010-05-16	21:21:33.2	+19:05:05.1	2.02	19.2	0.34	-169.8 ± 2.4
26	2010-05-16	21:21:39.0	+19:07:51.7	2.06	22.0	0.39	-152.9 ± 7.3
27	Combined	21:21:32.8	+19:10:02.8	3.04	19.4	0.32	-183.3 ± 2.3
	2009-11-16						-180.2 ± 2.9
	2010-05-16						-184.0 ± 2.4
28	2009-11-16	21:21:16.9	+19:06:32.8	3.37	21.4	0.35	-159.5 ± 6.7
29	2010-05-16	21:21:24.7	+19:03:52.9	3.49	21.0	0.28	-175.6 ± 7.9
30	2009-11-16	21:21:15.9	+19:05:25.4	3.92	20.7	0.27	-173.6 ± 4.8
31	Combined	21:21:31.2	+19:12:36.2	5.57	19.2	0.30	-153.5 ± 2.4
	2009-11-16						-156.9 ± 2.7
	2010-05-16						-151.8 ± 2.5
32	2009-11-16	21:21:05.8	+19:05:33.3	6.14	19.9	0.18	-169.6 ± 4.0

Note. Velocity error bars were determined from measurement overlaps as discussed in Section 2.2.

Table 2
Photometric and Kinematic Data for Keck/DEIMOS Sample—II. Non-members

ID	Date (yyyy-mm-dd)	α (J2000) (h m s)	δ (J2000) ($^\circ\ '\ ''$)	Radial Distance ($'$)	r (mag)	$(g-r)$ (mag)	$v_{\rm helio}$ (km s^{-1})
33	2009-11-16	21:21:33.9	+19:07:21.5	0.75	16.7	0.51	-60.6 ± 2.2
34	2009-11-16	21:21:27.9	+19:07:19.3	0.78	21.5	0.47	-237.3 ± 4.5
35	2009-11-16	21:21:32.7	+19:06:12.8	0.91	17.8	0.44	-54.9 ± 2.2
36	2009-11-16	21:21:34.6	+19:06:33.1	0.98	16.6	0.53	-96.6 ± 2.2
37	Combined	21:21:32.0	+19:08:02.5	1.04	19.8	0.25	-161.8 ± 2.6
	2009-11-16						-159.6 ± 3.1
	2010-05-16						-163.4 ± 2.9
38	Combined	21:21:28.4	+19:06:00.7	1.20	19.3	0.48	-171.7 ± 2.4
	2009-11-16						-171.0 ± 2.6
	2010-05-16						-172.3 ± 2.6
39	2009-11-16	21:21:32.3	+19:05:52.2	1.20	19.2	0.49	-163.3 ± 2.3
40	2009-11-16	21:21:27.6	+19:06:06.1	1.23	21.5	0.49	-353.7 ± 4.7
41	2009-11-16	21:21:34.0	+19:05:56.9	1.29	16.1	0.72	-35.1 ± 2.2
42	2009-11-16	21:21:29.6	+19:05:25.3	1.64	18.6	0.51	-79.9 ± 2.2
43	2009-11-16	21:21:25.3	+19:06:05.9	1.65	16.9	0.44	-22.0 ± 2.2
44	2009-11-16	21:21:36.0	+19:05:44.2	1.75	16.6	0.43	28.8 ± 2.2
45	2009-11-16	21:21:38.8	+19:07:10.0	1.84	21.2	0.41	-166.1 ± 6.2
46	2009-11-16	21:21:39.6	+19:06:14.2	2.19	18.5	0.54	-49.0 ± 2.2
47	2009-11-16	21:21:21.4	+19:07:26.6	2.31	16.1	0.56	-3.6 ± 2.2
48	2009-11-16	21:21:22.5	+19:08:12.6	2.33	16.3	0.54	-14.5 ± 2.2
49	2010-05-16	21:21:29.2	+19:09:26.9	2.45	19.4	0.48	-98.2 ± 2.3
50	2009-11-16	21:21:42.6	+19:07:08.1	2.74	19.0	0.34	-120.5 ± 2.4
51	2009-11-16	21:21:38.3	+19:04:46.0	2.84	17.8	0.39	3.2 ± 2.2
52	2010-05-16	21:21:25.9	+19:09:42.5	2.94	20.9	0.44	27.7 ± 5.2
53	2010-05-16	21:21:32.7	+19:04:02.1	3.03	17.4	0.36	-109.6 ± 2.2
54	2010-05-16	21:21:20.7	+19:05:11.9	3.05	18.5	0.49	-8.4 ± 2.2
55	2009-11-16	21:21:44.2	+19:07:35.6	3.16	19.4	0.37	-221.1 ± 2.5
56	2009-11-16	21:21:28.7	+19:10:13.1	3.23	18.3	0.42	-40.2 ± 2.3
57	2009-11-16	21:21:40.4	+19:04:28.4	3.39	18.4	0.53	-42.7 ± 2.2
58	2009-11-16	21:21:16.7	+19:06:33.2	3.40	21.3	1.17	25.7 ± 3.2
59	2009-11-16	21:21:24.4	+19:03:58.8	3.42	18.7	0.51	-31.3 ± 2.3
60	2009-11-16	21:21:43.3	+19:08:56.1	3.47	17.8	0.37	2.7 ± 2.2
61	2010-05-16	21:21:32.9	+19:10:29.3	3.48	19.8	1.15	-19.5 ± 7.1
62	2009-11-16	21:21:39.3	+19:04:06.2	3.53	19.0	0.37	-323.2 ± 2.4
63	2009-11-16	21:21:33.9	+19:10:30.8	3.55	17.1	0.43	-45.6 ± 2.2
64	2009-11-16	21:21:34.8	+19:03:30.9	3.63	18.3	0.37	-115.2 ± 2.3
65	2009-11-16	21:21:30.6	+19:10:43.4	3.69	19.5	0.46	-67.3 ± 2.3
66	2009-11-16	21:21:15.0	+19:06:31.5	3.82	16.4	0.48	6.6 ± 2.2
67	2009-11-16	21:21:29.9	+19:10:54.1	3.88	19.8	0.33	-300.6 ± 3.3
68	2009-11-16	21:21:14.2	+19:07:52.7	4.07	17.1	0.51	-89.6 ± 2.2
69	2009-11-16	21:21:47.5	+19:08:21.6	4.11	17.4	0.58	-69.4 ± 2.3
70	2009-11-16	21:21:22.7	+19:03:25.2	4.11	18.3	0.38	-113.2 ± 2.5
71	2009-11-16	21:21:38.9	+19:10:49.6	4.22	18.0	0.55	2.4 ± 2.2
72	2009-11-16	21:21:22.7	+19:03:15.4	4.25	20.7	0.81	-117.3 ± 2.8
73	Combined	21:21:37.6	+19:03:03.9	4.26	17.1	0.37	-160.6 ± 2.2
	2009-11-16						-160.7 ± 2.2
	2010-05-16						-160.6 ± 2.2
74	2010-05-16	21:21:35.1	+19:11:11.6	4.27	22.2	0.58	-331.8 ± 5.1
75	2010-05-16	21:21:34.4	+19:02:48.1	4.31	18.7	0.34	-274.2 ± 2.3
76	2009-11-16	21:21:48.0	+19:05:20.7	4.36	19.5	0.39	-97.4 ± 2.4
77	2009-11-16	21:21:26.9	+19:02:44.6	4.40	16.4	0.63	-19.4 ± 2.2
78	2010-05-16	21:21:23.4	+19:11:06.5	4.45	16.2	0.51	-30.9 ± 2.2
79	2009-11-16	21:21:34.1	+19:02:37.2	4.47	18.2	0.48	-83.2 ± 2.3
80	2009-11-16	21:21:13.1	+19:05:26.9	4.52	18.8	0.52	-39.1 ± 2.3
81	2009-11-16	21:21:35.5	+19:11:26.1	4.53	16.9	0.59	-62.8 ± 2.2
82	2009-11-16	21:21:11.8	+19:07:03.2	4.55	18.3	0.54	-90.0 ± 2.2
83	2009-11-16	21:21:49.8	+19:08:15.6	4.61	18.3	0.45	-76.6 ± 2.2
84	2009-11-16	21:21:12.5	+19:05:25.2	4.66	17.9	0.47	-71.9 ± 2.2
85	2009-11-16	21:21:11.1	+19:06:23.1	4.75	21.4	0.41	-162.4 ± 3.9
86	2010-05-16	21:21:38.7	+19:11:29.3	4.81	20.0	0.30	-177.3 ± 2.9
87	2009-11-16	21:21:29.9	+19:11:52.0	4.84	19.8	0.28	-239.4 ± 2.8
88	2009-11-16	21:21:39.2	+19:02:32.3	4.89	17.5	0.32	-75.9 ± 2.2
89	2010-05-16	21:21:22.7	+19:11:37.5	4.99	17.1	0.55	29.8 ± 2.2

Table 2
(Continued)

ID	Date (yyyy-mm-dd)	α (J2000) (h m s)	δ (J2000) (° ′ ″)	Radial Distance (′)	r (mag)	$(g-r)$ (mag)	$v_{\rm helio}$ (km s^{-1})
90	2009-11-16	21:21:31.1	+19:12:05.1	5.05	17.0	0.48	-39.3 ± 2.2
91	2010-05-16	21:21:22.5	+19:11:42.4	5.09	18.6	0.63	-23.7 ± 2.2
92	2010-05-16	21:21:22.5	+19:11:45.0	5.13	16.7	0.63	-54.1 ± 2.2
93	2009-11-16	21:21:40.9	+19:11:41.9	5.21	17.3	0.59	-30.0 ± 2.2
94	2009-11-16	21:21:52.9	+19:07:43.9	5.23	15.9	0.67	30.2 ± 2.2
95	2009-11-16	21:21:08.8	+19:07:14.0	5.24	21.4	0.44	-172.2 ± 9.6
96	2009-11-16	21:21:52.6	+19:05:42.5	5.27	20.9	0.31	-298.4 ± 6.9
97	2010-05-16	21:21:22.3	+19:02:02.0	5.40	18.2	0.45	-4.6 ± 2.2
98	2010-05-16	21:21:22.5	+19:12:03.4	5.41	21.6	1.01	-48.1 ± 5.6
99	2009-11-16	21:21:32.5	+19:12:26.7	5.42	18.0	0.32	-27.5 ± 2.2
100	2009-11-16	21:21:08.0	+19:06:54.5	5.44	18.6	0.45	-37.8 ± 2.3
101	2009-11-16	21:21:10.5	+19:09:40.1	5.51	20.7	0.35	-133.1 ± 3.7
102	2010-05-16	21:21:37.1	+19:01:34.1	5.65	20.9	0.31	-438.2 ± 4.4
103	2009-11-16	21:21:07.5	+19:08:45.9	5.81	17.5	0.55	-31.7 ± 2.3
104	2010-05-16	21:21:24.9	+19:01:22.3	5.84	17.6	0.48	-55.9 ± 2.2
105	2009-11-16	21:21:56.9	+19:05:50.4	6.23	16.3	0.53	-17.7 ± 2.2
106	Combined	21:21:28.7	+19:13:19.1	6.31	21.2	0.17	-284.5 ± 5.0
	2009-11-16						-297.5 ± 11.8
	2010-05-16						-282.2 ± 5.3
107	2009-11-16	21:21:57.5	+19:08:07.8	6.36	17.9	0.57	-55.7 ± 2.2
108	2010-05-16	21:21:33.0	+19:13:33.1	6.54	16.6	0.51	-21.3 ± 2.2
109	2009-11-16	21:21:56.5	+19:09:40.7	6.58	18.5	0.55	-55.7 ± 2.2
110	2010-05-16	21:21:28.3	+19:13:48.3	6.80	17.3	0.38	0.5 ± 2.2
111	2010-05-16	21:21:39.5	+19:00:31.0	6.82	16.6	0.55	-27.9 ± 2.7
112	2009-11-16	21:21:59.9	+19:07:31.5	6.85	17.1	0.44	-2.2 ± 2.2
113	2009-11-16	21:21:29.3	+19:13:53.3	6.87	17.1	0.64	-41.3 ± 2.2
114	2009-11-16	21:21:24.8	+19:13:44.8	6.87	16.7	0.41	-97.1 ± 2.2
115	2009-11-16	21:21:32.6	+19:13:59.2	6.96	17.1	0.38	-10.4 ± 2.2
116	2009-11-16	21:21:58.4	+19:09:41.7	7.01	17.0	0.60	6.2 ± 2.2
117	2009-11-16	21:22:01.1	+19:06:38.3	7.11	17.8	0.50	3.4 ± 2.2
118	2010-05-16	21:21:30.6	+19:14:09.9	7.13	16.1	0.48	-47.2 ± 2.2
119	2009-11-16	21:21:37.7	+19:14:06.8	7.25	18.6	0.46	-44.8 ± 2.3
120	2009-11-16	21:21:39.0	+19:14:22.4	7.58	17.8	0.49	-34.9 ± 2.2
121	2009-11-16	21:22:03.7	+19:06:59.6	7.72	18.6	0.32	-62.7 ± 2.3
122	2009-11-16	21:22:03.3	+19: 8:35.9	7.80	16.3	0.52	14.0 ± 2.2
123	2010-05-16	21:21:21.1	+19:14:48.2	8.11	18.2	0.44	-26.4 ± 2.5
124	2009-11-16	21:21:39.6	+19:14:54.8	8.14	21.3	0.24	-236.6 ± 5.9
125	2010-05-16	21:21:30.8	+19:15:12.7	8.18	18.5	0.48	6.2 ± 2.2
126	2009-11-16	21:21:39.5	+19:15: 1.9	8.25	18.3	0.46	-273.7 ± 2.3
127	2009-11-16	21:21:24.0	+19:15:26.8	8.57	18.2	0.63	-17.8 ± 2.2
128	2009-11-16	21:21:37.1	+19:15:40.8	8.77	18.4	0.35	-26.4 ± 2.3
129	2009-11-16	21:22: 8.7	+19: 7:42.4	8.94	17.9	0.41	-51.5 ± 2.2
130	2009-11-16	21:21:38.0	+19:15:56.8	9.07	18.0	0.34	-53.9 ± 2.2
131	2010-05-16	21:21:30.0	+19:16:21.1	9.32	17.6	0.54	-32.6 ± 2.3
132	2009-11-16	21:21:38.1	+19:16:18.5	9.42	18.7	0.41	-285.0 ± 2.4

Note. Velocity error bars were determined from measurement overlaps as discussed in Section 2.2.

the line-of-sight velocities for our full spectroscopic sample. We detect a clear overdensity of line-of-sight velocities which begin at the center of Seg 3, and continue out to ∼14 times the half-light radius of the system (26″, see Section 4.2). These stars exhibit an average systemic velocity of 167 km s^{-1}, and are offset by ∼150 km s^{-1} from the center of the Milky Way distribution at this position. We hypothesize that stars in our sample within 167 ± 30 km s^{-1} are candidate members of Seg 3. This velocity range is chosen to be wide enough to allow for the inclusion of extra-tidal stars, yet small enough to prevent the inclusion of significant numbers of Milky Way stars. We note, however, that our results are not sensitive to small changes in the size of this velocity window.

In Figure 2, we present the r versus $g-r$ CMD of stars within $5r_{1/2}$ of the center of Seg 3, using our IMACS photometry. Also plotted in the CMD are stars that are in our spectroscopic sample but lie at larger radii. We find a distinct main sequence of stars associated with Seg 3, with similar photometric properties as those found by Belokurov et al. (2010). An eyeball fit suggests that this main sequence of stars is well described by an isochrone with an age of 12 Gyr and [Fe/H] = −1.7 (Dotter et al. 2008), shifted by a distance modulus of 16.15. In Section 4.1, we consider the quality of fits for isochrones with different ages, metallicities, and distance moduli. While these may differ from the isochrone used here, we note selection of our member sample will not depend on small deviations in isochrone

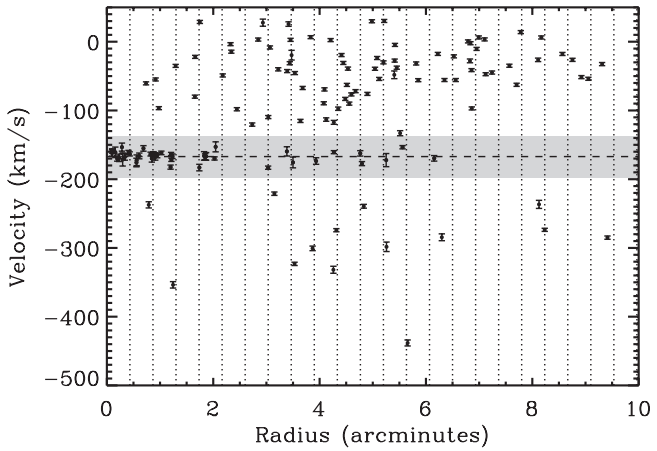

Figure 1. Line-of-sight velocities vs. distance from the center of Seg 3 for our entire spectroscopic sample. Vertical dotted lines represent radial steps in increments of $r_{1/2} = 26'$ (derived in Section 4.2). We detect a clear overdensity of points within $v \sim -167 \pm 30$ km s^{-1} (highlighted in gray), which we associate with Seg 3. The bulk of Milky Way stars lie in the velocity range ~ -125 to 25 km s^{-1}, more than 40 km s^{-1} away from the velocities of Seg 3.

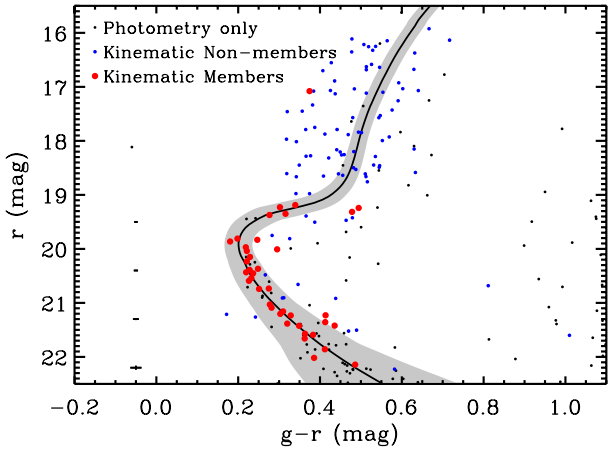

Figure 2. r vs. $g-r$ color–magnitude diagram of Segue 3. Small black points are stars within $5r_{1/2}$ of the center of Seg 3 for which only IMACS photometric data are available. Plotted at $g-r = -0.05$ are the average photometric uncertainties as a function of magnitude. Small blue (large red) points indicate stars with measured line-of-sight velocities that are outside (within) 30 km s^{-1} from the systemic velocity of Seg 3. The black curve represents the isochrone of a stellar population with an age of 12 Gyr and [Fe/H] $= -1.7$ (Dotter et al. 2008). We impose a color–magnitude selection indicated by the gray band, which roughly corresponds to 5σ photometric uncertainties about the isochrone. Our final list of candidate members for Seg 3 consists of all stars which pass our kinematic and photometric criteria (large red points, within gray band).

(A color version of this figure is available in the online journal.)

properties, since we select members using a wide $\sim 5\sigma$ CMD window.

We impose two selection criteria for probable Seg 3 members. First, we kinematically select stars that have line-of-sight velocities within 167 ± 30 km s^{-1}. Second, we require Seg 3 members to pass a photometric cut (gray area, Figure 2) which corresponds approximately to the 5σ average photometric uncertainty region around our fiducial isochrone. In total, we select 32 likely members of Seg 3 and in Figure 3 we present the spatial distribution of the members.

3.1. Foreground Contamination

Examining our sample of Seg 3 member stars, we find a number of stars which lie at large distances (up to $14r_{1/2}$)

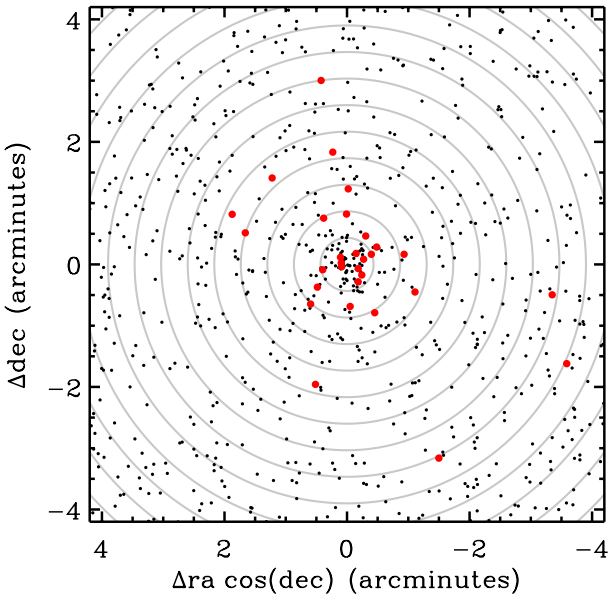

Figure 3. Spatial distribution of our spectroscopically confirmed members of Seg 3. Plotted in black are the locations of stars with color $g-r < 1.0$ for which we do not have spectroscopic coverage. Overplotted in red are the locations of identified Seg 3 members. Gray contours indicate increasing steps in the half-light radius of Seg 3. The apparently irregular distribution of red points reflects the non-uniform spectroscopic coverage, rather than a true irregularity in the underlying distribution of member stars.

(A color version of this figure is available in the online journal.)

from the center of Seg 3. We consider the possibility that these stars, and those at smaller radii, might instead be foreground Milky Way contaminants. To estimate the degree of foreground contamination in our member sample, we utilize the Besancon model of the Milky Way (Robin et al. 2003). The estimate does not include possible contamination in our Seg 3 member sample from halo substructures or from unbound stars that are physically associated with Seg 3.

For our estimation we select all Besancon stars that are within one degree of the center of Seg 3, and are within a 10σ average photometric uncertainty region about our fiducial isochrone (a factor two larger than for our Seg 3 members). Of these stars, we find that the number of stars that meet our above kinematic criteria is $3.66\% \pm 0.18\%$ of those that do not. In our spectroscopic sample we find 11 stars that satisfy CMD criteria but are not within our kinematic window, implying an average of 0.40 ± 0.02 stars are contaminating our sample of Seg 3 members. From this average, we quantify the frequency of larger numbers of contaminants using Poisson statistics. We find that $N = \{1, 2, 3, 4\}$ contaminants occur with a frequency of $\{26.2, 5.52, 0.78, 0.06\}\%$. Thus, we conclude that the likely number of Milky Way field halo contaminants is $\leqslant 2$ at $\sim 95\%$ confidence.

4. PHOTOMETRIC ANALYSIS OF SEGUE 3

4.1. Stellar Population

We now use our spectroscopically selected members to derive the age, [Fe/H], and distance of Seg 3, using a maximum likelihood method which closely follows that described by Frayn & Gilmore (2002). For the procedure, a suite of isochrones are fit to a sample of stars, assigning to each a bivariate Gaussian probability function whose variance is set by the associated photometric errors. We apply this analysis using all stars in our

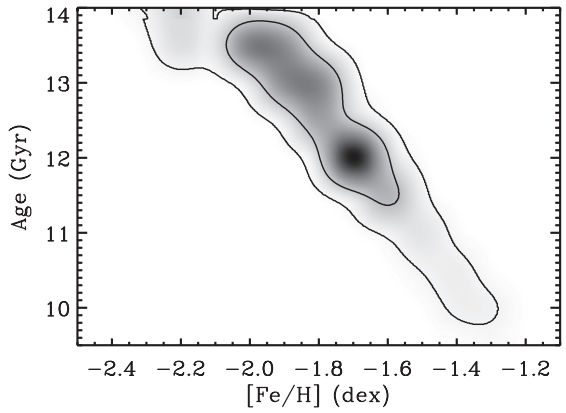

Figure 4. Smoothed maximum likelihood joint probability density in age–metallicity space for all Segue 3 stars within a radius of 39′, combined with 17 spectroscopically confirmed stars that lie outside that area. Contour lines show the 1σ and 2σ confidence levels. The diagonal flow of the contour lines reflects the age–metallicity degeneracy inherent to such an isochrone fitting procedure. The 1D marginalized parameters around the best fit are age $= 12.0^{+1.5}_{-0.4}$ Gyr, [Fe/H] $= -1.7^{+0.07}_{-0.27}$ dex, and $m - M = 16.14 \pm 0.09$ mag.

photometric data within a radius 39′ from the object's center ($r_{1/2}$ from Belokurov et al. 2010), to which we add the 17 spectroscopically confirmed member stars that lie outside that area, resulting in a total sample of 125 stars.

For a given isochrone i we compute the likelihood

$$\mathcal{L}_i = \prod_j p(\{g, g-r\}_j | i, \{g, g-r\}_{ij}, \mathrm{dm}_{0,i}), \quad (1)$$

where

$$p(\{g, g-r\}_j | i, \{g, g-r\}_{ij}, \mathrm{dm}_{0,i}) = \frac{1}{\sqrt{2\pi}\sigma_{g_j}\sigma_{(g-r)_j}} \times \exp\left(-\frac{1}{2}\left[\left(\frac{g_j - (g_{ij} + \mathrm{dm}_{0,i})}{\sigma_{g_j}}\right)^2 + \left(\frac{(g-r)_j - (g-r)_{ij}}{\sigma_{(g-r)_j}}\right)^2\right]\right). \quad (2)$$

For each star, j, $\{g, g-r\}_{ij}$, and $\mathrm{dm}_{0,\mathrm{i}}$ are, respectively, the magnitude, color, and de-reddened distance modulus values for isochrone i that maximize the likelihood of the entire data set $\{g, g-r\}_j$ in Equation (2). We take an approximate solution to finding the values of $\{g, g-r\}_{ij}$ and $\mathrm{dm}_{0,i}$ by searching over a series of fine steps in g, $g-r$, and dm_0 values for each isochrone. Input isochrones are supplied by the Dartmouth library (Dotter et al. 2008), and interpolated so g, $g-r$ values step by 0.001 mag in the two-dimensional (2D) color–magnitude space. The distance modulus $\mathrm{dm}_0 = m - M$ is sampled over a range of $15.0 < \mathrm{dm}_0 < 17.0$ in steps of 0.01 mag.

We calculate the maximum likelihood values $\mathcal{L}_i$ over a grid of isochrones, covering an age range from 8 to 14 Gyr and metallicity range $-2.5 \leqslant$ [Fe/H] $\leqslant -0.9$ dex. Grid steps are 0.5 Gyr in age and 0.1 dex in [Fe/H]. With a grid of $\mathcal{L}_i$ values, we can locate the most likely value and compute confidence intervals by interpolating between grid points. In addition to this interpolation, we smooth the likelihood values over ∼2 grid points in order to provide a more conservative estimate of parameter uncertainties. In Figure 4, we present the relative density of likelihood values for the sample described above. We find that the isochrone with the highest probability has an age of 12.0 Gyr and [Fe/H] $= -1.7$, with 68% and 95% confidence contours presented in the figure. The marginalized uncertainties about this most probable location correspond to an age of $12.0^{+1.5}_{-0.4}$ Gyr, a metallicity of [Fe/H] $= -1.7^{+0.07}_{-0.27}$ dex, and a distance modulus of $\mathrm{dm}_0 = 16.14 \pm 0.09$ mag ($d = 16.9 \pm 0.7$ kpc). We assume a distance of 17 kpc in the calculation of physical size and absolute magnitude in Section 4.2.

To assess how much the inclusion of the 17 spectroscopic members outside of 39′ has influenced the above results, we repeat the above computation using only the 32 spectroscopic members found above. We find that parameters derived for this subsample are consistent with the larger sample but have larger uncertainties, with age $= 13.5^{+1.5}_{-1.3}$ Gyr, [Fe/H] $= -1.9^{+0.20}_{-0.39}$ dex, and $\mathrm{dm}_0 = 16.08 \pm 0.13$ mag ($d = 16.4 \pm 1.0$ kpc).

4.2. Structural Parameters

We present a new determination of the structural parameters of Seg 3, using the photometry presented in Section 2.1. For our analysis we follow the maximum likelihood method of Martin et al. (2008), as described in Muñoz et al. (2010). This method starts by assuming an analytic surface density profile, and then fits the profile parameters using all stars meeting CMD criteria, thus avoiding the need to bin or smooth data. We fit structural parameters for Seg 3 using two choices of density profiles commonly used to describe the light distribution in ultra-faint systems, an exponential and a Plummer (Plummer 1911) profile. In both cases, the parameters we calculate are the scale length of the system, the coordinates of its center, its ellipticity, position angle, and the foreground/background stellar density. To estimate parameter uncertainties, we carry out a bootstrap analysis using 10^4 realizations of the photometric data.

Before proceeding with our analysis of the structure of Seg 3, we must carefully consider which photometric data to use. We note in Section 2.1 that the 90% completeness limit of our data is at a magnitude of ∼23.8 for g and r filters. However, due to the increased contamination of unresolved galaxies beyond a magnitude of $r \sim 23$, we conservatively limit our structural analysis to stars brighter than $r \sim 22.5$. In Table 3, we present the results for both Plummer and exponential density profiles. We find structural parameters very similar to those of Belokurov et al. (2010), with most results within 1σ of values previously reported. A notable exception, however, is our determination of the half-light radius of $r_{1/2} = 28' \pm 8'$ and $26' \pm 5'$, or 2.2 ± 0.7 pc and 2.1 ± 0.4 pc for an exponential and Plummer profile, respectively. While within $\sim 1.5\sigma$ from the value of Belokurov et al., these are ∼30% smaller than previously found. We attribute such discrepancies to our higher quality photometric data, and to the different analysis techniques used here. In Figure 5, we present the 1D surface density profile and 2D surface brightness contours for Seg 3. Both the Plummer and exponential profiles are found to provide good fits to the data, while 2D contours reveal a circularly symmetric profile, with little evidence for strong tidal distortion.

In addition to structural properties, we estimate the absolute magnitude of Seg 3 following the method described in Muñoz et al. (2010). Previous estimates of the absolute magnitude by Belokurov et al. (2010) reported a value of $M_V = -1.2$ for Seg 3. Such a low magnitude makes traditional methods for calculating total luminosities, such as adding individual stellar fluxes, too sensitive to the inclusion (or exclusion) of potential members (outliers; e.g., Walsh et al. 2008; Martin et al. 2008; Muñoz et al. 2010). To alleviate issues related to low number statistics, the method used here relies solely on the total number

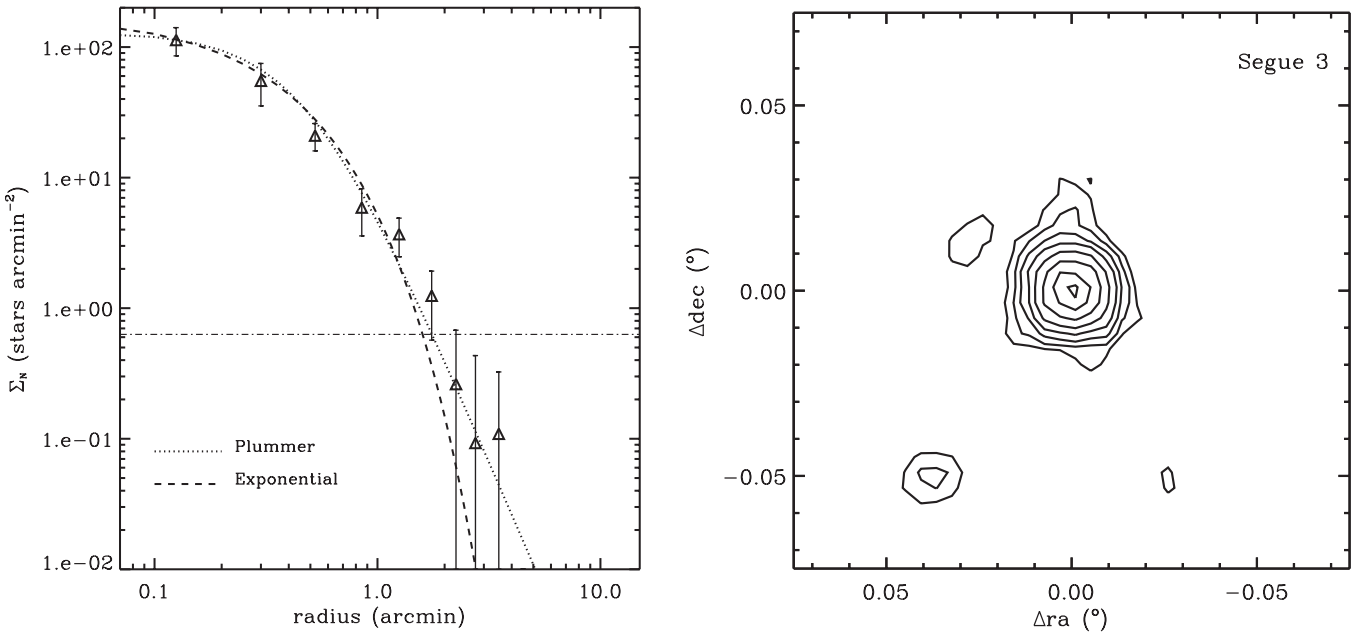

Figure 5. Left: 1D surface density profile of Seg 3 for a Plummer and exponential profile, both of which provide acceptable fits to the data. The dot-dashed line represents the surface density of background stars inferred by our analysis. Right: 2D surface brightness contours for Seg 3. Contour levels are $\{3, 5, 8, 12, 18, 26, 36, 44\}\sigma$ fainter than the peak surface brightness, where 5σ is 2.35 mag arcmin^{-1} fainter than the peak value of $\mu_{0,V} = 24.1$ mag arcmin^{-1} (assuming a Plummer profile). We find that the stellar distribution is approximately circularly symmetric until it falls to levels comparable to the background.

Table 3
Structural Parameters for Segue 3

Quantity	Symbol	Value
Exponential Profile		
Right ascension	α_0	21:21:31.05 ± 1.″6
Declination	δ_0	+19:07:02.6 ± 2.″4
Half-light radius (″)	$r_{1/2}$	28 ± 8
Half-light radius (pc)[a]		2.2 ± 0.7
Ellipticity	ϵ	0.24 ± 0.14
Position angle	θ	25° ± 17°
Number of stars[b]	N_*	65 ± 6
Absolute magnitude[a]	M_V	−0.06 ± 0.78
Central surface brightness	$\mu_{V,0}$	$23.9^{+1.0}_{-0.8}$ mag arcmin^{-1}
Plummer Profile		
Right ascension	α_0	21:21:31.02 ± 1.″8
Declination	δ_0	+19:07:03.7 ± 2.″6
Half-light radius (″)	$r_{1/2}$	26 ± 5
Half-light radius (pc)[a]		2.1 ± 0.4
Ellipticity	ϵ	0.23 ± 0.11
Position angle	θ	33° ± 36°
Number of stars[b]	N_*	64 ± 6
Absolute magnitude[a]	M_V	−0.04 ± 0.78
Central surface brightness	$\mu_{V,0}$	$24.1^{+1.0}_{-0.8}$ mag arcmin^{-1}

Notes.
[a] Using a distance of 17 kpc for Segue 3.
[b] For stars with $r < 22.5$ mag.

of stars that belong to the satellite and not on their individual magnitudes.

In short, our method estimates the absolute magnitude by integrating a theoretical luminosity function, using the above structural analysis. Following the results of Section 4.1, we use a luminosity function for a 12 Gyr stellar population with an [Fe/H] = −1.7 from Dotter et al. (2008), assuming a Salpeter initial mass function (IMF). We then integrate this luminosity function down to the magnitude limit of $r = 22.5$, and scale the results to match the number of stars found by our structural analysis. Our final estimate of the absolute magnitude, therefore, is the integral of this scaled luminosity function, integrated down to the limiting mass of the Salpeter IMF ($0.1 M_\odot$). Like our structural parameters, the uncertainty of the absolute magnitude is estimated by bootstrapping the data 10^4 times. This method yields $M_V = -0.06 \pm 0.78$ or $L_V = 90^{+95}_{-56}\ L_\odot$ for an exponential profile. If we use a Plummer profile instead, we obtain $M_V = -0.04 \pm 0.78$ which translates into $L_V = 89^{+93}_{-45}\ L_\odot$. While the uncertainties are significant, these values make Segue 3 the lowest luminosity stellar system known to date. This tiny luminosity combined with the small size of Seg 3 yields a brighter central surface brightness ($\mu_{0,V} = 23.90^{+1.0}_{-0.8}$ for an exponential profile, $\mu_{0,V} = 24.10^{+1.0}_{-0.8}$ for a Plummer profile) than that of the most diffuse Milky Way companions.

We note, in fact, that our values for the luminosity and surface brightness of Seg 3 may be overestimated if stars fainter than the magnitude limit of our observations have been preferentially lost due to relaxation (see Section 6). While it is unclear whether relaxation is significant in Seg 3, such an effect would result in only a small change in our estimates, since low-mass stars do not contribute much to the total luminosity. For the remainder of the analysis presented here, we adopt the structural parameters and absolute magnitude obtained from using a Plummer profile above.

5. SEGUE 3: A PROBABLE STAR CLUSTER

We assess the nature of Segue 3 through several independent lines of evidence. First, in Section 5.1 we examine the velocity distribution of Seg 3 spectroscopic members. In Section 5.2, we consider possible spreads in the distribution of ages and metallicities of Seg 3 spectroscopic member stars. Finally, in Section 5.3 we examine the size and luminosity of Seg 3 relative to other known Milky Way satellites. As discussed below, we conclude that all three indicators agree with our null hypothesis:

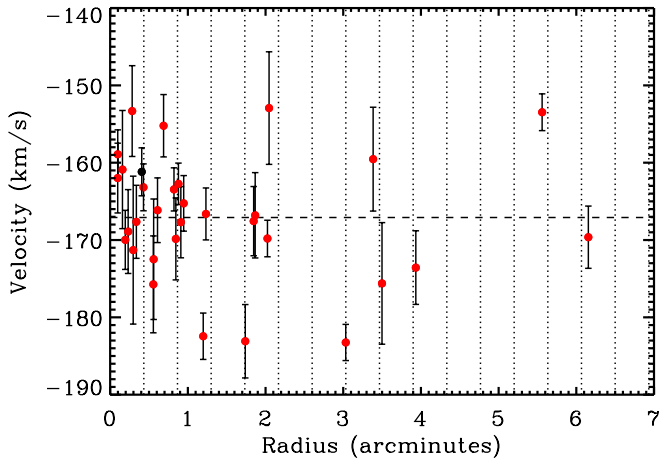

Figure 6. Line-of-sight velocities of members vs. distance from the center of Seg 3. Plotted in black is the combined velocity for the binary star found in our repeat measurements (described in Section 2.2). The dashed line indicates the systemic velocity at -167 km s^{-1}, while the dotted lines indicate increasing steps in $r_{1/2}$ from the center.

(A color version of this figure is available in the online journal.)

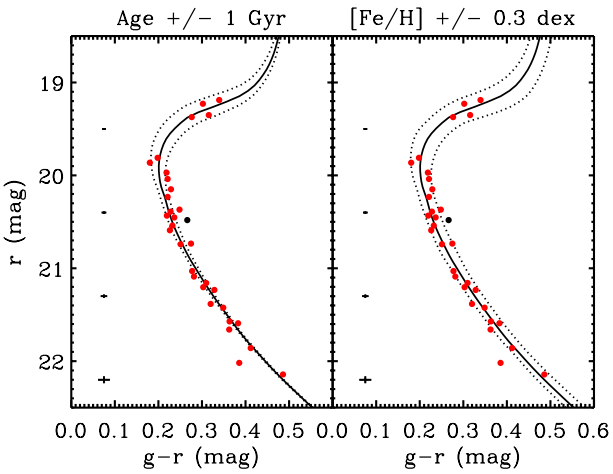

Figure 7. Color–magnitude diagram from Figure 2, showing only member stars of Seg 3. The black point indicates the color and magnitude of the binary star found with repeat velocity measurements (see Section 2.2). Average photometric uncertainties are plotted on the left in each panel. The solid, black curve represents our fiducial isochrone from Figure 2. In the left panel, dotted curves show the isochrones for a stellar population which are older by $\pm$1 Gyr. In the right panel, dotted curves show the isochrones for a stellar population with [Fe/H] values which differ by $\pm$0.3 dex. Within the photometric uncertainties, the members of Seg 3 are consistent with a spread in age ([Fe/H]) less than 1 Gyr (0.3 dex).

(A color version of this figure is available in the online journal.)

Segue 3 is an old, extremely low luminosity star cluster in the halo of the Milky Way.

5.1. Velocity Distribution

We present in Figure 6 the distribution of velocities for Seg 3 spectroscopic members. We find that the majority of the members (66%) lie at small projected radii ($\leqslant 3r_{1/2}$), with the remainder up to 14 half-light radii from the center of Seg 3. We consider these 11 spatially outlying stars, as well as other lines of evidence, as possible signs of stellar mass loss in Seg 3 (discussed below in Section 6).

To obtain a reasonable estimate of the velocity dispersion (and hence dynamical mass) of Seg 3, we choose to focus on the velocity measurements within $3r_{1/2}$ only, and exclude the binary star identified by repeat velocity measurements (ID 9, Table 1). This choice excludes distant candidate member stars potentially unbound to Seg 3, and reduces the amount of foreground contamination, since foreground stars are more likely at larger radii. In estimating the velocity dispersion, we use the maximum likelihood technique described by Walker et al. (2006).

If we naively include all 20 stars within $3r_{1/2}$, we infer a velocity dispersion of 5.3 ± 1.3 km s^{-1} for Seg 3. However, this relatively large dispersion is primarily driven by the presence of a single outlying star (ID 20, Table 1), with a measured velocity of -182 ± 3 km s^{-1}, $\sim 5\sigma$ away from the systemic velocity of Seg 3. Omitting this star, our estimate of the velocity dispersion plummets to 1.2 ± 2.6 km s^{-1}, a value consistent with zero.

Inclusion of the outlying star has a profound consequence on the nature of Seg 3. If included, we must necessarily infer the presence of significant amounts of dark matter in Seg 3, since the velocity dispersion would imply a mass-to-light ratio of 645^{+1286}_{-442} within $r_{1/2}$.[7] If omitted, the velocity distribution allows very small values of the dispersion, giving dynamical masses consistent with stellar material alone. We must, therefore, carefully consider whether to omit the outlying star.

We use Monte Carlo simulations to test the hypothesis that the outlying star is revealing the true velocity dispersion, rather than being a genuine outlier from the velocity distribution. First, we assume a value for the true, intrinsic velocity dispersion of Seg 3 ranging from 0 to 10 km s^{-1}. We then repeatedly generate a sample of 20 stars with velocities drawn randomly from a Gaussian corresponding to the intrinsic dispersion, convolved with our DEIMOS measurement uncertainties. Of these samples, we take those which have a dispersion between 5.3 ± 1.3 km s^{-1} and ask how frequently the dispersion is reduced to below 3.8 km s^{-1}, once we omit the largest outlier. Our simulations indicate that the highest frequency occurs at an intrinsic dispersion of 5.8 km s^{-1}, at a rate of 3.8%. Therefore, at $>$95% confidence, our simulations indicate that the outlying star within $3r_{1/2}$ is not due to low-number statistics, but is instead a genuine outlier from the distribution. With this conclusion, we assume that it is reasonable to omit the outlying star, and infer a velocity dispersion of 1.2 ± 2.6 km s^{-1} within $3r_{1/2}$. By adopting such a velocity dispersion, we can infer a mass-to-light ratio of 33^{+156}_{-144} within $r_{1/2}$.[7] While inconclusive, from this mass-to-light ratio alone there is no compelling evidence for significant dark matter content in Segue 3.

5.2. Age and Metallicity

Properties of the stellar populations of Milky Way satellites have proven to be a useful indicator for the presence of an underlying dark matter halo. In short, the deeper potential well provided by non-baryonic material enables star formation processes to withstand feedback effects from, e.g., supernovae, facilitating more extended episodes of star formation. This effect manifests itself in the presence of a range of metallicities among stars, since metals from earlier generations of stars may be incorporated into subsequent ones. Ultra-faint satellites have demonstrated this phenomenon, showing internal [Fe/H] spreads up to 0.5 dex or more (Simon & Geha 2007; Kirby et al. 2008, 2011; Simon et al. 2011; Willman et al. 2011).

In Figure 7, we present the effect of varying the age and metallicity of isochrones from our fiducial values of 12 Gyr and

[7] Using the mass estimator of Wolf et al. (2010), assuming a constant velocity dispersion within $3r_{1/2}$.

[Fe/H] = −1.7. In the right panel, we see that the members of Seg 3 are consistent with a spread in [Fe/H] < 0.3 dex, within the photometric errors. Such dispersions in [Fe/H] are smaller than values typically found in ultra-faint systems (Frebel et al. 2010; Kirby et al. 2011), indicating the stellar population of Seg 3 may be quite different from dark matter dominated satellites.

In addition to internal spreads in metallicity, the average value of [Fe/H] in stars can also be used to test whether Seg 3 may contain significant dark matter. Kirby et al. (2011) show a strong correlation between the total luminosity and [Fe/H] for Milky Way dwarf galaxies, such that the faintest satellites are the most metal poor. Extrapolating the relation from Kirby et al., we find Seg 3, with an absolute magnitude of $M_V \sim 0.0$, should exhibit a mean [Fe/H] < −3.0, far lower than the $-1.7^{+0.07}_{-0.27}$ dex we observe. For comparison, Segue 1 ($M_V \sim -1.5$) has a value of [Fe/H] ∼ − 2.5 (Simon et al. 2011). For this to be a meaningful comparison, we assume that Seg 3 would not have undergone massive stellar loss if it contains significant dark matter.

The low spread and (relatively) high mean of [Fe/H] values inferred from isochrone comparisons indicate that the metallicity characteristics of Seg 3 are distinct from that of dark matter dominated ultra-faint satellites. While enticing, several caveats exist. First, our sample of Seg 3 members is small, totaling 32 stars. More extensive samples might show larger scatter than seen here. In addition, significant uncertainties exist in the values of theoretical isochrones, especially under the correlated effects of varying age and [Fe/H] values. We have only explored one such set of isochrones here (Dotter et al. 2008). To avoid such uncertainties, a definitive measurement of the metallicity would require spectroscopic measurements of [Fe/H] values. For our current data, this would require a calibration of the relationship between [Fe/H] and the Ca II triplet for main-sequence stars. Since no such relation exists, we do not attempt to relate the values of the Ca II triplet in our spectra to [Fe/H]. Nevertheless, we note that the scatter in Ca II equivalent width is consistent with no abundance spread.

5.3. Size and Luminosity

A final diagnostic tool for discriminating star clusters from satellites with dark matter halos is the relationship between size and luminosity of Milky Way objects. In Figure 8, we show the sizes and luminosities of Milky Way halo objects (distances >15 kpc). Of these systems we consider two classes, stellar systems with dark matter (dwarf spheroidal, ultra-faint dwarf galaxies) and those without dark matter (e.g., globular clusters). A clear trend is present between the two: at fixed luminosity, objects with dark matter are consistently larger in size, often by up to an order of magnitude, than objects classified as star clusters. Segue 3's size and luminosity are far smaller than those of objects known to be dominated by dark matter. This difference provides additional circumstantial evidence that Seg 3 is a star cluster. Such a conclusion is further supported by theoretical arguments, which expect low-mass dwarf galaxies to be significantly larger in size (e.g., Bullock et al. 2010) than Seg 3.

Under the three lines of evidence presented in this section, we conclude that Segue 3 is likely a star cluster with little to no dark matter content. This hypothesis is further supported by tentative signs for stellar mass loss (see below), which has also been seen in the majority of small and faint stellar clusters.

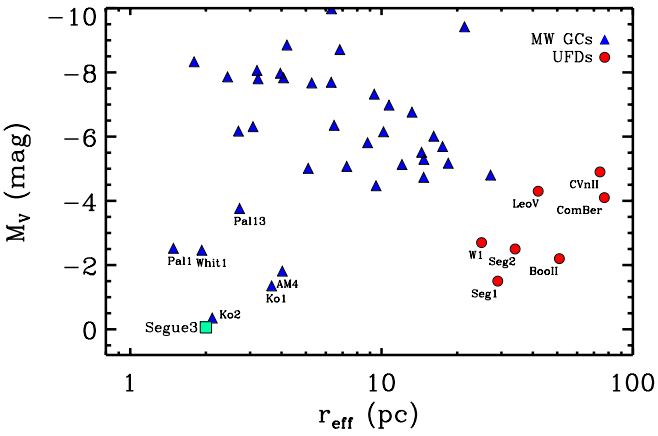

Figure 8. Size and luminosity of Milky Way halo objects (>15 kpc), presented as the effective radius and absolute *V*-band magnitude, respectively. At fixed luminosity, objects with significant dark matter (ultra-faint and dwarf spheroidal galaxies) are larger in size by up to an order of magnitude. Moreover, faint ($M_V < -4$) star clusters show effective radii <10 pc in size.

(A color version of this figure is available in the online journal.)

6. THE DYNAMICAL STATE OF SEGUE 3

Discussed in Section 5.1, the distribution of velocities within $3r_{1/2}$ of the center of Segue 3 implies a velocity dispersion of 1.2 ± 2.6 km s^{-1}. The distribution of these velocities is consistent with being drawn from a Gaussian distribution, suggesting that Seg 3 is bound within $3r_{1/2}$.

Although it is not possible to draw a robust conclusion about the extended stellar distribution of this extremely low luminosity system, if we consider Seg 3 members across all radii, then we find tentative evidence for mass loss in Seg 3. The fact that 1/3 of our candidate member stars lie outside of three half-light radii hints that there may be an excess of Seg 3 member stars at large distances, as expected if it is currently undergoing stellar mass loss. We attempted to quantify this excess (or lack thereof) by correcting the surface density profile of spectroscopic members for target efficiency and comparing with expectations from a pure Plummer model. However, uncertainty owing to small number statistics in both our characterization of target efficiency (as a function of position), and in our predicted number of stars at large radii, was too great to make a meaningful comparison with observations.

Of the 13 stars at radii $>2.5r_{1/2}$, four (IDs 20, 22, 27, and 31 in Table 1) lie at velocities more than 10 km s^{-1} away from the systemic velocity of -167.1 ± 1.5 km s^{-1}. Three of the four stars have velocities which are each ∼16 km s^{-1} below the systemic velocity of Seg 3, while the fourth has a velocity ∼14 km s^{-1} above the systemic. In a sample of 32 stars, the likelihood of finding four such stars in a tidally isolated system is small. Performing similar Monte Carlo tests as in Section 5.1, we determine these outlying stars are not due to small sample size at >99% confidence. These stars may be stars lost by Seg 3 and heated up by a dynamical interaction, or they may be contaminants from the field halo or from the possible proximity of Seg 3 to another known halo overdensity (see Section 7). However, simple estimates presented in Sections 3.1 and 7 indicate the chance of all four stars being contaminants is excluded at >99% confidence.

While such simple estimates may underestimate the degree of contamination of our member sample, mass loss in Seg 3 is nevertheless supported from dynamical arguments. First, we consider the possibility of tidal stripping in Seg 3 by

estimating the Jacobi radius r_J of the system. Since $r_J \propto M_{MW}^{-1/3}$, we conservatively overestimate r_J by assuming a Milky Way circular velocity of only 180 km s^{-1} at the Galactocentric distance of Seg 3 (10 kpc). This yields a value of $r_J = 10.4$ pc, ∼5 times the half-light radius of Seg 3. Given that Seg 3 is likely not on a purely circular orbit, and may be associated with a local overdensity (see below), the true tidal radius of Seg 3 is likely smaller still. Thus, from these simple estimates, it seems highly likely that Seg 3 is undergoing some sort of tidal stripping.

In addition to tidal stripping, we consider potential evidence for relaxation in Seg 3, using the half-mass relaxation time t_{rh} (Spitzer & Hart 1971; Gnedin & Ostriker 1997). Using our measurements of the structural properties of Seg 3 and assuming a Coulomb logarithm of $\ln(\Lambda) = \ln(0.02N)$, we estimate $t_{rh} = 144^{+153}_{-53}$ Myr. The timescale for total disruption of a cluster through relaxation is of order 10–50t_{rh} (see, e.g., Gnedin et al. 1999), implying an evaporation time of ∼1–7 Gyr for Seg 3. Such evaporation times are short relative to the estimated age of the stellar population (12 Gyr), indicating Seg 3 must have experienced significant mass loss in order to have survived to present day. Definitive support for relaxation can be obtained if signs of mass segregation are found in the system. Unfortunately, we are not able to see any clear signs of mass segregation, due to the small size and mass range (∼0.2 $M_\odot$) of our member sample.

Interestingly, the mass loss implied by the small tidal radius and small relaxation time of Seg 3 are similar to that found in other faint stellar systems (Koposov et al. 2007; Carraro 2009; Carraro et al. 2007; Niederste-Ostholt et al. 2010). For instance, Koposov et al. (2007) estimate Koposov 1 and 2 have $t_{rh} \sim 70$ and 55 Myr, and $r_J \sim 11$ and 9 pc, respectively. These facts, and the tentative associations to large-scale Galactic structures (see below), may indicate a common evolutionary history for these systems.

7. PROXIMITY TO KNOWN STELLAR HALO STRUCTURE

Segue 3 lies at a distance of ∼17 kpc from the Sun, at a location of $(l, b) = (69.4, -21.27)$. This is coincident in projection with the recently discovered Hercules–Aquila cloud (Belokurov et al. 2007). Early discovery data (SDSS DR5) presented by Belokurov et al. indicated that the cloud is located at $l \approx 40°$, and extends Galactic latitudes as low as −40 at $l \sim 50°$.

Arguments for the spatial overlap of Seg 3 and extended halo substructure have been strengthened by the analysis of SEGUE/DR7 SDSS data by de Jong et al. (2010). Subtracting off a smooth model for the stellar distribution, de Jong et al. find a number of new halo overdensities. Of these, one lies at $(l, b, D_{helio}) = (70°, -22° \pm 1°, 15 \pm 1$ kpc), in excellent agreement with the location of Seg 3. While coincident with the Hercules–Aquila cloud in projection, the distance to stars in this newly identified halo structure (and in Seg 3) is closer than the >20 kpc distances of the Hercules–Aquila debris in that direction. It is presently unclear whether or not these structures all have a common origin.

Although Seg 3 appears to be coincident with a spatially extended de Jong et al. (2010) halo overdensity, this halo overdensity is not necessarily kinematically associated with Seg 3. There is a dearth of (non-member) stars with velocities ±45 km s^{-1} from the systemic velocity of Seg 3, suggesting that this structure may not be kinematically associated with Seg 3. As shown in Figure 1, we find a significant number of stars with large negative velocities, more than 40 km s^{-1} lower than the systemic velocity of Seg 3. These stars are not associated with any other known Milky Way structure, and may be attributed to the de Jong et al. (2010) $(l, b) = (70°, -22°)$ overdensity. It is unlikely that these stars are instead Hercules–Aquila stars because their color–magnitude distribution is consistent with a more nearby stellar population than the Hercules–Aquila cloud in this direction.

If we assume the stars in this kinematic halo structure are normally distributed, we find their distribution has mean of −290 km s^{-1} and FWHM of 48 km s^{-1}. Under this assumption, we would expect to find an average of ∼0.2 stars that meet our velocity criterion for membership in Seg 3 (cf. Section 4). Accounting for Poisson variance, therefore, we expect this low velocity population of stars (<−200 km s^{-1}) may be contaminating our Seg 3 member sample by at most one star (99% CL). Thus, given our contamination estimates for both the MW foreground and for this additional kinematic halo population, we can rule out contamination from these source as the origin for *all* four outliers in Section 6 at >99% confidence.

Other faint stellar systems (like Koposov 1) have also been linked to large streams and structures (Frinchaboy et al. 2004; Carraro et al. 2007; Koposov et al. 2007; Carraro 2009; Forbes & Bridges 2010). Because of the two distinct halo kinematic populations in our data, it is unclear whether Seg 3 is associated with the de Jong et al. (2010) $(l, b) = (70°, -22°)$ overdensity. It seems likely that Seg 3 is kinematically offset from this overdensity. A more extensive photometric–kinematic study of the halo debris in this region of sky might be able to reach a more robust conclusion about the association, or lack thereof, of Seg 3 and other halo structures.

8. CONCLUSIONS

We have investigated the nature of the faint Milky Way satellite Segue 3 using new Keck/DEIMOS spectroscopic and Magellan/IMACS photometric data. Using the data we have identified a sample of 32 probable member stars for Seg 3, one of which is definitively identified as a binary system through repeated velocity measurements. We summarize our conclusions as follows.

1. New IMACS photometry reveals a distinct main sequence of stars in the CMD of Seg 3, with the majority of these stars lying within two half-light radii of the center. Using maximum likelihood methods which fit isochrones from Dotter et al. (2008), we infer an average age of $12.0^{+1.5}_{-0.4}$ Gyr and an average [Fe/H] of $-1.7^{+0.07}_{-0.27}$ for the stellar population.
2. We analyze the structural properties of Seg 3, using Plummer and exponential profiles. We find structural parameters similar to those of Belokurov et al. (2010), except for the half-light radius which we find to be smaller by ∼30%. Using a Salpeter IMF and CMD properties from our photometry, we find that Seg 3 has an absolute magnitude of $M_V = 0.0 \pm 0.8$, making it the faintest stellar system known to date.
3. Examining 20 spectroscopic member stars within three half-light radii, we find a kinematically bound group of 19 member stars and identify one star which is an outlier of the velocity distribution (at 95% confidence). For this

group of bound stars we infer a velocity dispersion of 1.2 ± 2.6 km s^{-1}, consistent with very low values for the true velocity dispersion.

4. Segue 3 is likely a faint stellar cluster with no significant dark matter content. This is evidenced by our measurement of the velocity dispersion within three half-light radii, the (relatively) high average and low scatter in [Fe/H] values implied by isochrones, and small physical size of Seg 3 relative to similar luminosity ultra-faint dwarf galaxies.
5. We find signs of possible mass loss in Segue 3, indicated by 11 candidate member stars outside of $3r_{1/2}$. While these stars may originate from the Milky Way or nearby substructure, we estimate a Jacobi radius of $r_J < 5r_{1/2}$ and a half-mass relaxation time of $t_{rh} \sim 150$ Myr for Seg 3, suggesting mass loss should be important.
6. Seg 3 appears spatially coincident with an extended overdensity discovered by de Jong et al. (2010), which may be associated with the Hercules–Aquila cloud. However, we find that it is kinematically offset from the structure; evidenced by the low density of non-member stars within ± 45 km s^{-1} from the systemic velocity of Seg 3. In our spectroscopic sample we identify a collection of stars with line-of-sight velocities <200 km s^{-1}, which may be associated with the structure. We find that at most one star from this population may be misidentified as a member.

R.F. and B.W. acknowledge support from NSF AST-0908193. M.G. acknowledges support from NSF grant AST-0908752 and the Alfred P. Sloan Foundation. R.R.M. acknowledges support from the GEMINI-CONICYT Fund, allocated to the project N°32080010. G.S.D.C. acknowledges research support in part through Australian Research Council Discovery Projects Grant DP0878137. This paper includes data gathered with the 6.5 m Magellan Telescopes located at Las Campanas Observatory, Chile. Australian access to the Magellan Telescopes was supported through the National Collaborative Research Infrastructure Strategy of the Australian Federal Government. Some of the data presented herein were obtained at the W. M. Keck Observatory, which is operated as a scientific partnership among the California Institute of Technology, the University of California, and the National Aeronautics and Space Administration. The Observatory was made possible by the generous financial support of the W. M. Keck Foundation. This research has also made use of NASA's Astrophysics Data System Bibliographic Services.

REFERENCES

Belokurov, V., Evans, N. W., Bell, E. F., et al. 2007, ApJ, 657, L89
Belokurov, V., Walker, M. G., Evans, N. W., et al. 2010, ApJ, 712, L103
Bertin, E. 2006, in ASP Conf. Ser. 351, Astronomical Data Analysis Software and Systems XV, ed. C. Gabriel et al. (San Francisco, CA: ASP), 112
Bertin, E., & Arnouts, S. 1996, A&AS, 117, 393
Bertin, E., Mellier, Y., Radovich, M., et al. 2002, in ASP Conf. Ser. 281, Astronomical Data Analysis Software and Systems XI, ed. D. A. Bohlender, D. Durand, & T. H. Handley (San Francisco, CA: ASP), 228
Bullock, J. S., Stewart, K. R., Kaplinghat, M., Tollerud, E. J., & Wolf, J. 2010, ApJ, 717, 1043
Carraro, G. 2009, AJ, 137, 3809
Carraro, G., Zinn, R., & Moni Bidin, C. 2007, A&A, 466, 181
de Jong, J. T. A., Yanny, B., Rix, H., et al. 2010, ApJ, 714, 663
Dotter, A., Chaboyer, B., Jevremović, D., et al. 2008, ApJS, 178, 89
Faber, S. M., Phillips, A. C., Kibrick, R. I., et al. 2003, Proc. SPIE, 4841, 1657
Forbes, D. A., & Bridges, T. 2010, MNRAS, 404, 1203
Frayn, C. M., & Gilmore, G. F. 2002, MNRAS, 337, 445
Frebel, A., Simon, J. D., Geha, M., & Willman, B. 2010, ApJ, 708, 560
Frinchaboy, P. M., Majewski, S. R., Crane, J. D., et al. 2004, ApJ, 602, L21
Gnedin, O. Y., Lee, H. M., & Ostriker, J. P. 1999, ApJ, 522, 935
Gnedin, O. Y., & Ostriker, J. P. 1997, ApJ, 474, 223
Harris, W. E. 1996, AJ, 112, 1487
Kirby, E. N., Lanfranchi, G. A., Simon, J. D., Cohen, J. G., & Guhathakurta, P. 2011, ApJ, 727, 78
Kirby, E. N., Simon, J. D., Geha, M., Guhathakurta, P., & Frebel, A. 2008, ApJ, 685, L43
Koposov, S., de Jong, J. T. A., Belokurov, V., et al. 2007, ApJ, 669, 337
Marigo, P., Girardi, L., Bressan, A., et al. 2008, A&A, 482, 883
Martin, N. F., de Jong, J. T. A., & Rix, H.-W. 2008, ApJ, 684, 1075
Muñoz, R. R., Geha, M., & Willman, B. 2010, AJ, 140, 138
Niederste-Ostholt, M., Belokurov, V., Evans, N. W., et al. 2010, MNRAS, 408, L66
Plummer, H. C. 1911, MNRAS, 71, 460
Robin, A. C., Reylé, C., Derrière, S., & Picaud, S. 2003, A&A, 409, 523
Simon, J. D., & Geha, M. 2007, ApJ, 670, 313
Simon, J. D., Geha, M., Minor, Q. E., et al. 2011, ApJ, 733, 46
Sohn, S. T., Majewski, S. R., Muñoz, R. R., et al. 2007, ApJ, 663, 960
Spitzer, L., Jr., & Hart, M. H. 1971, ApJ, 164, 399
Stetson, P. B. 1987, PASP, 99, 191
Walker, M. G., Mateo, M., Olszewski, E. W., et al. 2006, AJ, 131, 2114
Walsh, S. M., Willman, B., Sand, D., et al. 2008, ApJ, 688, 245
Willman, B., Geha, M., Strader, J., et al. 2011, AJ, in press (arXiv:1007.3499)
Wolf, J., Martinez, G. D., Bullock, J. S., et al. 2010, MNRAS, 406, 1220